Journal of
METAMORPHIC GEOLOGY

J. metamorphic Geol., 2017, **35,** 197–211 doi:10.1111/jmg.12228

Geochronological challenges posed by continuously developing tectonometamorphic systems: insights from Rb–Sr mica ages from the Cycladic Blueschist Belt, Syros (Greece)

R. A. CLIFF,[1] C. E. BOND,[2] R. W. H. BUTLER[2] AND J. E. DIXON[3,*]
[1]*School of Earth and Environment, University of Leeds, Leeds LS2 9JT, UK (b.cliff@earth.leeds.ac.uk)*
[2]*School of Geosciences, University of Aberdeen, Meston Building, Aberdeen AB24 3UE, UK*
[3]*School of Geosciences, University of Edinburgh, The King's Buildings, James Hutton Road, Edinburgh EH9 3FE, UK*

ABSTRACT Is metamorphism and its causative tectonics best viewed as a series of punctuated events or as a continuum? This question is addressed through examination of the timing of exhumation of the Cycladic Blueschist Belt (CBB). The cause of scatter beyond analytical error in Rb–Sr geochronology was investigated using a suite of 39 phengite samples. Rb–Sr ages have been measured on phengite microsamples drilled from specific microstructures in thin sections of calcschists and metabasites from the CBB on Syros. The majority are from samples that have well-preserved blueschist facies mineral assemblages with limited greenschist facies overprint. The peak metamorphic temperatures involved are below the closure temperature for white mica so that crystallization ages are expected to be preserved. This is supported by the coexistence of different ages in microstructures of different relative age; in one sample phengite from the dominant extensional blueschist facies fabric preserves an age of 35 Ma while post-tectonic mica, millimetres away, has an age of 26 Ma. The results suggest that micro-sampling techniques linked to detailed microstructural analysis are critical to understanding the timing and duration of deformation in tectonometamorphic systems. North of the Serpentinite Belt in northern Syros, phengite Rb–Sr ages are generally between 53 and 46 Ma, comparable to previous dates from this area. South of the Serpentinite Belt phengite in blueschist facies assemblages associated with extensional fabrics linked to exhumation have ages that range from 42 Ma down to *c.* 30 Ma indicating that extensional deformation while still under blueschist facies conditions continued until 30 Ma. No age measurements on samples with unambiguous evidence of deformation under greenschist facies conditions were made; two rocks with greenschist facies assemblages gave phengite ages that overlap with the younger blueschist samples, suggesting blueschist facies phengite is preserved in these rocks. Two samples yielded ages below 27 Ma; one is from a post-tectonic microstructure, the other from a greenschist in which the fabric developed during earlier blueschist facies conditions. These ages are consistent with previous evidence of greenschist facies conditions from *c.* 25 Ma onwards. The data are consistent with a model of deformation that is continuous on a regional scale.

Key words: blueschist; exhumation; phengite; Rb–Sr ages; Syros.

INTRODUCTION

Considerable progress has been made in improving the analytical quality of geochronological data from metamorphic belts and the range of ages determined now commonly greatly exceeds the analytical uncertainties. Often the data are evaluated in the framework of an episodic model and supposed excess scatter in ages is attributed to poorly understood 'geological error' (e.g. incomplete resetting of the isotope system). This begs the question; is the geological history of an orogenic belt best described as a series of distinct, discrete 'events' or as an evolving continuum of processes? The validity of 'event-based' approaches is uncertain given continually changing conditions of temperature, pressure, fluid availability and deformation. Temperature, pressure and stress variations are undoubtedly continuous but the response of individual rocks may be discontinuous as strain migrates within a rock pile and crystallization of minerals may be further limited by kinetic considerations such as fluid access. In addition the geochemical systems used to determine mineral ages may be disturbed by various processes after crystallization. The challenge is to define how far detailed information on the timing and rates of tectonic processes can be recovered from rocks and what scales of sampling are needed to achieve valid results. The

*Deceased.

area investigated in this study is the northern part of Syros in the Cycladic Blueschist Belt (CBB) of Greece. The aim was to clarify the duration of blueschist facies metamorphism, and the timing of subsequent greenschist facies overprinting and its relationship with deformation during exhumation.

A hierarchy of conditions must be met to ensure a measured age has a well-defined relationship with a specific stage in the tectonometamorphic evolution. Rock samples must have clearly defined relationships to structures at outcrop and larger scales. They must also be free of weathering effects that would compromise the geochemical integrity of the material dated – a challenge when the clearest field relations are often seen in slightly weathered outcrops. Samples must also have minerals suitable for dating, ideally as part of mineral assemblages that tightly constrain the *P–T* conditions of crystallization. The analysed minerals must further have textural/microstructural relationships that tie back to structures observed in the field. A consequence of this hierarchy is that few samples meet all these necessary criteria so that a wide range of field and petrographic investigation is required as prelude to rather few age measurements.

Which minerals/methods are potentially useful and what are their limitations?

The choice of which dating method is best to optimize the usefulness of the ages measured involves a balance between a number of considerations including analytical precision and accuracy of the method, the minerals on which they can be used and their susceptibility to disturbance after crystallization. Uranium–lead dating of various accessory minerals offers the greatest analytical precision but presents some of the greatest challenges in tying the mineral crystallization to the overall reaction history and other aspects of sample development. Progress has been made in tying monazite crystallization to deformation (Erickson *et al.*, 2015) or reaction history using zoning in individual dated grains (e.g. Mottram *et al.*, 2015). Garnet can be tied to metamorphic crystallization history in great detail through its chemical zoning and mineral inclusions and it can be dated by Lu–Hf and/or Sm–Nd, but results can be distorted by the presence of refractory inclusions (e.g. Scherer *et al.*, 2000; Anczkiewicz & Thirlwall, 2003). Minerals such as mica offer clear relationships to deformation history through their involvement in fabric development. Much effort has been expended on dating mica using ^{40}Ar–^{39}Ar (e.g. Putlitz *et al.*, 2005). However, this method is susceptible to argon loss at relatively low temperatures and there are issues with the lack of controls on what, if any, radiogenic argon is incorporated from ambient fluids at the time of crystallization. Excess argon, leading to spuriously high ages, has been found in both biotite and white mica in various metamorphic settings (e.g. Roddick *et al.*, 1980; Warren *et al.*, 2012; Smye *et al.*, 2013).

Rb–Sr dating of phengitic white mica is the focus of this paper, so it is important to examine the issues involved with use of this system in more detail. The Rb–Sr system in white mica closes at higher temperatures than Ar. No experimental data on Sr diffusion in white mica are available so that no quantitative estimates of the likely scale of diffusive re-equilibration can be made. However, more recent age distribution patterns suggest closure temperature as much as 100 °C higher than the canonical 500 °C often cited (cf. Jäger *et al.*, 1967; Villa, 1998). For example, the white mica Rb–Sr ages in Cliff *et al.* (1985) include ages of 220 Ma in Permo-Carboniferous protoliths, implying only ~30% resetting in rocks that experienced peak Alpine metamorphic temperatures ~630 °C (Droop, 1985) for several million years.

For the calcite- and epidote-bearing samples analysed here the complications from varying modal proportions discussed by Jenkin *et al.* (1995) are unlikely to be important because only a small proportion of the rock Sr is contained in phengite (see later). Moreover, data on Sr diffusion in calcite (Cherniak, 1997 – $\sqrt{D}t \gg 1$ mm at 500 °C for million year timescales) suggest radiogenic Sr from exchange with phengite would be easily dispersed in surrounding calcite grains. Rb–Sr ages from phengite are only reliable if the composition of Sr incorporated when it crystallized can be determined. Defining this composition is complicated by the distribution of Sr among several minerals that possess a wide range of diffusion properties and distinct closure temperatures. Minerals with high closure temperatures may be excluded from the reservoir contributing Sr to the mica while those with lower closure temperatures, as a result of later exchange, may not extrapolate back to the composition they had when phengite crystallized. Thus the composition of Sr available to a growing phengite may differ from that of the whole rock at the time of crystallization.

Active deformation and reaction of all major Sr-bearing minerals will promote equilibration of phengite with the rest of the rock (e.g. calcschists of the Entrelor Shear Zone of the Western Alps; Freeman *et al.*, 1997). In weakly deformed rocks containing high closure temperature feldspar, the scale of equilibration can be localized below thin-section scale (cm), even under amphibolite facies conditions (e.g. Cliff & Meffan-Main, 2003). Where multiple generations of white mica are present, later generations may grow in exchange with a reservoir depleted in radiogenic Sr compared to the whole rock because of isolation of earlier formed mica (Sousa *et al.*, 2013). To obtain reliable ages in these situations it is necessary to identify and analyse the specific mineral/s that effectively approximate the Sr isotopic characteristics of the reservoir from which mica grew. For example, Cliff & Meffan-Main (2003) obtained consistent dates

by analysing low-Rb/Sr minerals in the same microstructural setting as the dated phengite grains. The microsampling approach used in that work was adopted here to examine how far it can provide tighter constraints on the timing of specific stages in a prolonged, possibly continuous, exhumation and deformation history on Syros.

Syros as a case study for dating structural development

Syros is located in the centre of the CBB in the Aegean (Fig. 1, inset). Models for the blueschist terrane focused initially on exhumation of the high-*P* rocks in the footwall to a major low-angle fault (e.g. Lister *et al*., 1984; Jolivet *et al*., 1998). However, there is a continuing debate on the mechanisms of exhumation (e.g. Trotet *et al*., 2001; Bond *et al*., 2007; Philippon *et al*., 2011; Soukis & Stockli, 2013) and the role of penetrative strain during exhumation for the Cycladic blueschists. Through petrographic studies Trotet *et al*. (2001) argued for linked shear zones operating at greenschist facies that overprint deformation fabrics developed under blueschist and eclogite facies. Rosenbaum *et al*. (2002) argued that significant horizontal extension happened under blueschist conditions, overprinted by simple shear zones at greenschist facies conditions. These papers contrast with the conclusions of Keiter *et al*. (2004), who argued that there is no penetrative deformation on Syros after peak metamorphism. This led to the conclusion that, as in earlier models (Lister *et al*., 1984; Jolivet *et al*., 1998), exhumation of Syros was accommodated by a major detachment exhuming the blueschist rocks passively. These debates have continued with authors arguing for heterogeneous coaxial extension through eclogite–blueschist to greenschist facies (Bond *et al*., 2007; Philippon *et al*., 2011 and others).

The use of geochronology to elucidate the timing and continuity, or otherwise, of the development of deformation structures observed in the field and petrographically has been the focus of several studies over the last 10 years (e.g. Bröcker & Enders, 1999; Forster & Lister, 2005; Bröcker & Keasling, 2006; Fu *et al*., 2010; Bröcker *et al*., 2013). Even with the extent and diversity of geochronological studies in the Cyclades and specifically on Syros (Table S1), the question remains as to how effectively we can date the metamorphic events and their associated deformation histories. This study clarifies some of the issues involved.

GEOLOGY OF SYROS

Syros consists of two distinct metamorphic rock terranes (Fig. 1). In the SE of the island the albitic gneiss of the Vari Unit shows no evidence of high-*P* metamorphic conditions and is believed to represent older continental basement (Philippon *et al*., 2011). Philippon *et al*. (2011) have the Vari Unit as

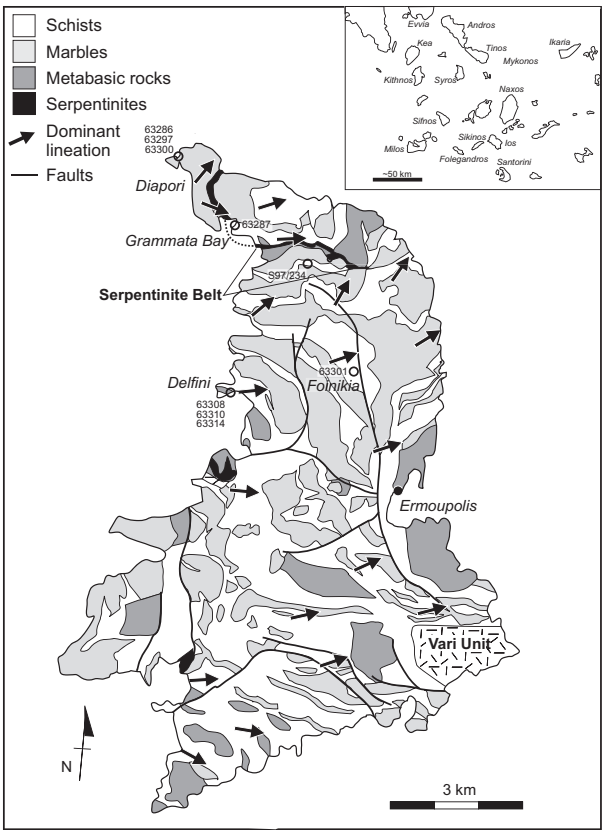

Fig. 1. Geological map – modified from Bond *et al*. (2007); inset shows the central location of Syros within the Cyclades.

basement underlying the high-*P* rocks above, whereas Trotet *et al*. (2001), Soukis & Stockli (2013), Laurent *et al*. (2016) and others interpret this unit as an upper tectonic sheet, carried onto high-*P* rocks by a regionally extensive, low-angle extensional detachment fault.

In contrast, the rocks beneath the detachment, termed the Ermoupolis Unit, are younger. The Ermoupolis Unit includes metabasic rocks from basaltic and gabbroic protoliths, with tracts of serpentinite, believed to be remnants of the Tethyan oceanic crust (e.g. Bonneau, 1984). However, most of this unit consists of metasedimentary rocks including pelitic schists, psammites, conglomerates and marble. The marbles can be traced across the island over several kilometres (Fig. 1; e.g. Ridley, 1982). The Ermoupolis Unit was metamorphosed to eclogite–blueschist facies (Dixon, 1976; Dixon *et al*., 1987; Okrusch & Bröcker, 1990). Peak metamorphic conditions are generally estimated to lie in the epidote–blueschist/eclogite stability field, at ~20 kbar and 500–550 °C (e.g. Trotet *et al*., 2001; Schumacher *et al*., 2008).

The eclogite–blueschists are variably retrogressed to greenschist facies across the island (e.g. Trotet *et al*., 2001; Bond *et al*., 2007). For Trotet *et al*. (2001), the different degrees of preservation of blueschists in the Attic-Cyclades reflect different *P–T*

paths that relate spatially to the position of deeply penetrating extensional shear zones. However, different degrees of retrogression occur on a variety of scales, from kilometres (e.g. Trotet *et al.*, 2001) to hand specimen (Bond *et al.*, 2007). The greenschist facies overprint strongly relates to fluid infiltration on the neighbouring island of Sifnos (Fig. 1, inset; Schliestedt & Matthews, 1987; Ganor *et al.*, 1989). Bond *et al.* (2007) argued that greenschist facies metamorphism on Syros is also fluid driven and often associated with contiguous deformation in localized zones. These deformation zones often became 'locked' by the formation of albite porphyroblasts as greenschist facies retrogression continued (Bond *et al.*, 2007), further localizing deformation. However, the extent of penetrative down-pressure deformation structures and their role in the exhumation of the high-*P* terrane is controversial. Keiter *et al.* (2004) and Brady *et al.* (2004) noted the widespread preservation of calcite pseudomorphs after aragonite within high-*P* blueschist bodies, suggesting in these areas that there has been no penetrative ductile deformation below the stability field for aragonite, for which Keiter *et al.* (2004) place the lower pressure limit at ~12 kbar for their *P–T* path. These authors argue that no pervasive ductile strain was recorded on Syros below pressures of 12 kbar. On the other hand, Philippon *et al.* (2013) reported lawsonite pseudomorphs were deformed in the greenschist facies.

The timing of key parts of the tectonometamorphic history of the Attic-Cycladic blueschists, in general and for Syros specifically is also controversial. Cretaceous ages of 80–75 Ma, derived from U–Pb dating of zircon from omphacite, in eclogitic meta-igneous rocks of the Ermoupolis Unit are interpreted to date peak metamorphism (Bröcker & Enders, 1999). Other workers (e.g. Keiter *et al.*, 2004) presume they relate to the age of the sea floor, or hydrothermal metasomatism in a subduction zone (Bröcker & Keasling, 2006). In contrast, geochronology from across the Cyclades utilizing Ar–Ar, Rb–Sr dating of white mica, Lu–Hf dating of garnet and metamorphic zircon growth give Eocene ages in the range of (*c.* 53–40 Ma) for peak metamorphism and an Oligocene–Miocene age (*c.* 25–18 Ma) for greenschist facies metamorphism (Bröcker *et al.*, 2004). Bröcker *et al.* (2004) highlighted that many of the Ar–Ar cooling ages are older than the Rb–Sr white mica ages for the same rocks, a good indicator of contamination by 'excess' radiogenic argon. Bröcker *et al.* (2004) also identified significant discrepancies in the Rb–Sr mica geochronology suggesting isotopic disequilibrium at the sample scale. A comprehensive review of previous geochronology is summarized in Table S1.

ANALYTICAL TECHNIQUES

Oriented samples were collected from outcrops where the relationship with structures and fabrics were clear, in most cases from areas for which Bond *et al.* (2007) presented detailed structural data. Based on hand specimen examination, samples with significant amounts of white mica related to either blueschist or greenschist facies fabrics were collected.

Conventional oriented thin sections were prepared and examined to confirm mineral assemblage, textural relationships and presence of suitable size phengite grains for microdrilling. From an initial suite of 30 hand specimens, 15 were selected for further study. The 150 μm thick polished sections, mounted in Crystalbond® were prepared from the selected samples and examined in the SEM. Grains of phengite suitable for microdrilling were identified based on size, lack of inclusions and/or evidence of alteration; the coordinates of the selected grains were recorded and transferred to scanned images of the entire section. Nine sections were found to be potentially suitable for microsampling and isotopic analysis. The Medenbach microscope drill used in this study isolates microsamples of adjustable diameter (0.1 to >1 mm) by removing an annulus of material around the targeted grain which can then be removed from the section for analysis. In some cases the sites selected using the SEM images proved unsatisfactory/unsuccessful for microdrilling: in these cases alternative microsamples were drilled with only optical images to guide sample selection.

Microsamples were processed in Class 10 workstations using a mixed ^{87}Rb–^{84}Sr spike. Sr was separated using Sr-Resin (Eichrom) and Rb by cation exchange in hydrochloric acid. Sr isotopic compositions were measured statically on a Thermo-Finnigan Triton while Rb was measured on a VG Micromass 30. Further details of the procedures are given in Appendix S1.

Ages and their uncertainties were determined using Isoplot-Ex 3.76 (Ludwig, 2012) including correlation coefficients where significant. For the small amounts of Sr analysed from some phengite grains the isobaric correction for Rb at mass 87 is a significant source of error. The uncertainties and error correlations were determined using a Monte Carlo simulation, which includes error contributions from this source and blank.

SAMPLES

Sampling localities are indicated in Fig. 1. The detailed localities and rock types in the following account follow the report of Bond *et al.* (2007). Results from five distinct locations in northern Syros are presented here and discussed in turn.

Gria Spilia (Grammata Bay)

Sample 63287 – calcschist containing calcite–phengite–garnet–dolomite–glaucophane–quartz–epidote–titanite. This sample was collected a few metres from

carbonate boudins showing the prismatic structure attributed to original crystallization as aragonite. Phengite is generally parallel to schistosity in discrete grains and felted aggregates (Fig. 2a). Glaucophane fractured during extension has the cracks infilled by carbonate. Six approximately fabric-parallel phengite microsamples (Fig. 3a,b) were extracted together with four calcite microsamples, one of which appeared to be altered.

Diapori

Three samples of the calcschist matrix of a strongly deformed, dominantly carbonate conglomerate were studied.

Sample 63286 – the mineral assemblage is calcite–phengite–glaucophane–quartz–albite. Calcite occurs as large grains enclosing phengite: many grains have bent twins and some have patchy extinction. Phengite occurs as single grains and felted aggregates parallel to schistosity (Fig. 2b) and occasionally as randomly oriented aggregates that may be pseudomorphic replacements of an earlier mineral. Four microsamples of fabric-parallel phengite and one from a randomly oriented aggregate (Fig. 3c) were extracted together with two calcite microsamples to constrain initial Sr composition.

Sample 63297 – contains calcite–phengite–glaucophane–epidote–quartz–albite. Phengite occurs as discrete grains and felted aggregates parallel to schistosity (Fig. 2c). Calcite grains are generally larger than the phengite, often elongated parallel to fabric and showing bent twins, undulose extinction and/or sub-grain development. Albite occurs as large anhedral grains associated with phengite. Five phengite microsamples were extracted; four were typical fabric-parallel grains/aggregates while the fifth (Ph1) was from an aggregate of grains at a high angle to the fabric, which was wrapped by fabric-parallel grains (Fig. 3d). Three calcite microsamples (Cc1–3) spatially associated with phengite (Ph1–3 respectively) were analysed.

Sample 63300 – contains calcite–phengite–glaucophane–chlorite–quartz–albite. Calcite occurs mainly as large twinned grains with highly irregular grain boundaries. Phengite is generally parallel to schistosity as discrete grains and felted aggregates (Fig. 2d) but there are also composite 'augen' in which phengite has a decussate texture associated with calcite and albite. Four microsamples of typical fabric-related phengite were extracted. One microsample of calcite was analysed together with a dilute acid leach of one of the microsamples which had adhering calcite prior to leaching.

Several samples were collected from the intensely deformed, dominantly greenschist, rocks immediately above the conglomerate. The relationship of these samples to the conglomerate samples is shown in Fig. S1. None of these contained phengite suitable for microsampling but their textures reveal important evidence that deformation continued into the greenschist facies. Sample 63298 has albite porphyroblasts which include blue amphibole grains some of which define earlier fabrics at a high angle to the external greenschist facies fabric (Fig. 2j,k). In 63299 albite porphyroblasts are ellipsoidal, showing undulose extinction and partially converted to a mosaic of subgrains (Fig. 2l).

Delfini

Sample 63310 – blueschist containing epidote–glaucophane–phengite–calcite–quartz–albite–titanite–tourmaline–chlorite. Glaucophane has extensional fractures infilled by carbonate; generally there is no sign of glaucophane instability adjacent to cracks suggesting it was stable during extension. Very rare glaucophane grains have minor chlorite at the margins. Phengite occurs as felted aggregates parallel to schistosity, sometimes together with calcite filling pressure shadows around larger epidote grains (Fig. 2e). Extractable phengite grains were small and analyses were made on two microsample composites – Ph1 + 2 + 5 and Ph7 + 8; all were aligned in the schistosity. Three epidote and two calcite microsamples were also analysed.

Sample 63314 – blueschist containing phengite–glaucophane–quartz–epidote–titanite–chlorite–albite–calcite–apatite. Glaucophane is zoned with darker blue rims: some grains have extensional cracks and in a few cases needles of the darker blue glaucophane have grown into the cracks from the original grain (Fig. 2f). Some titanite grains have an internal fabric defined by orientated small phengite grains at a high angle to the external schistosity (Fig. 2g). The majority of phengite grains are elongated and strongly aligned in the schistosity, but there are also more equant grains many of which are at high angles to the schistosity. Elongate epidote grains are well aligned in the schistosity. Eight phengite microsamples from typical aggregates were extracted but SEM images show small epidote inclusions are common (Fig. 3f); where possible adhering epidote was eliminated during transfer. One microsample each of epidote and apatite was analysed together with two grains of titanite (+phengite inclusions, Fig. 3e).

Foinikia

Sample 63301 – greenschist containing quartz–phengite–chlorite–albite–calcite–dolomite–titanite–apatite–paragonite. The shape of some albite grains suggests they have replaced pre-existing sheet silicate grains. Others are intergrown with chlorite in aggregates with overall shapes suggesting they replaced garnet. Phengite occurs mainly as felted aggregates parallel to schistosity (Fig. 2i) but also in decussate aggregates associated with albite in a possible

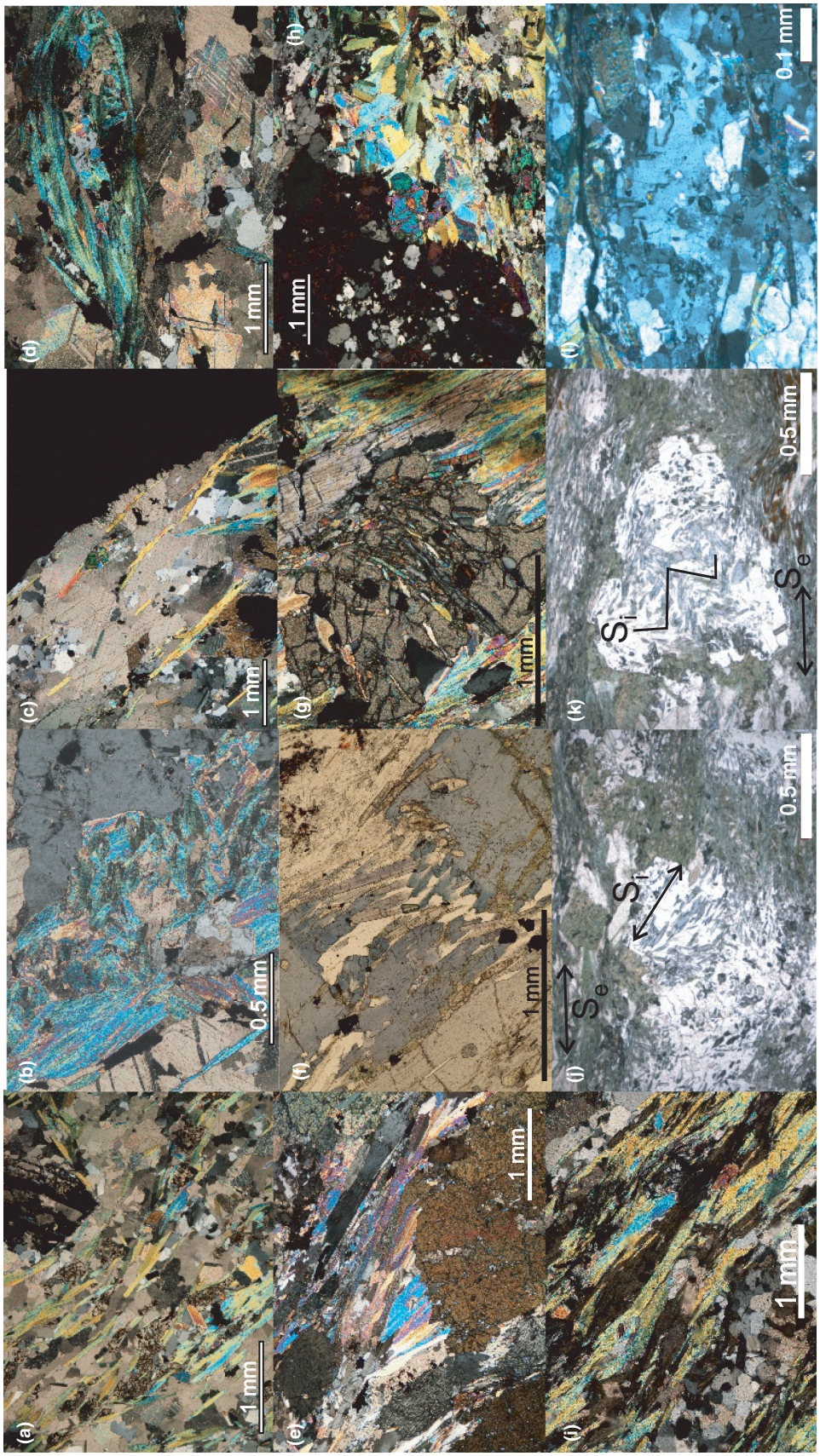

Fig. 2. Sample petrography. (a) 63287 view showing phengite aligned in the extensional fabric, calcite is the dominant mineral with a single garnet at the top of the image (x-polars). (b) 63286 view of phengite-rich area with a mixture of fabric-parallel and cross-cutting phengite, the latter in contact with albite (x-polars). (c) 63297 view showing phengite aligned in the extensional fabric together with calcite and minor quartz (x-polars). (d) 63300 view showing a cluster of phengite grains surrounded by calcite (x-polars). (e) 63310 aligned phengite and larger epidote grains (x-polars). (f) 63314 detail of extensional crack in a large glaucophane with fine-grained, darker blue amphibole in the crack fill. (g) 63314 titanite with aligned phengite inclusions at a high angle to the external fabric defined by the surrounding phengite grains (x-polars). (h) S97/234 decussate phengite grains in pressure shadow of garnet (now a chlorite pseudomorph) (x-polars). (i) 63301 phengite aligned in the extensional fabric (x-polars). (j) 63298 albite grain containing aligned glaucophane grains (S_i) at high angle to the surrounding greenschist facies schistosity (S_e). (k) 63298 albite grain with a crenulated glaucophane S_i surrounded by uncrenulated greenschist. (l) 63299 deformed albite in greenschist showing strained extinction and partial recrystallization.

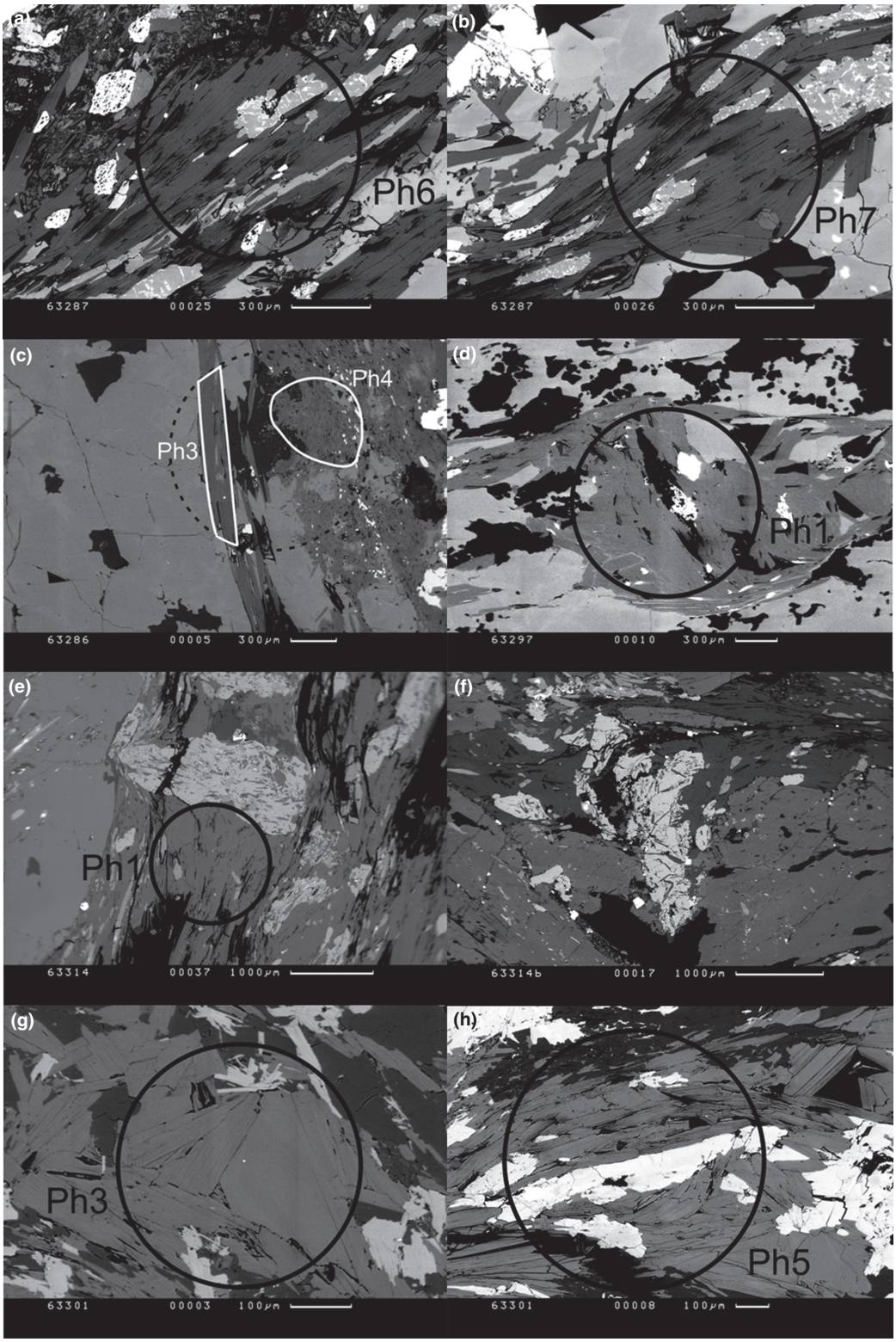

Fig. 3. Back-scattered electron images of selected phengite grains with microsample locations. Dated microsamples identified by the number after the decimal point. (a) Fabric-parallel phengite 63287.7. (b) Fabric-parallel phengite 63287.6. (c) Two generations of phengite; 63286.3 parallel to fabric and 63286.4 post-tectonic aggregate. (d) Pre-fabric phengite 63297.1, wrapped by later grains parallel to fabric. (e) Phengite parallel to fabric in titanite pressure shadow 63314.1. (f) Titanite with phengite inclusions in 63314b. (g) Late decussate phengite 63301.3. (h) Phengite parallel to fabric 63301.5

pseudomorph. In the polished thick section there is an 8 × 5 mm unfoliated area composed of randomly oriented phengite–paragonite–quartz and calcite. Five phengite microsamples were analysed, two from the randomly oriented area (Ph1, Ph7), a composite of two fabric-parallel grains (Ph5 + 5a, Fig. 3h) and one from a decussate cluster (Ph3, Fig. 3g) within the main fabric. Two microsamples of calcite and two of titanite were analysed.

Northern Oros Syringas

Sample S97/234 – greenschist containing albite–chlorite–phengite–epidote–quartz–calcite. Very rare traces of blue amphibole are enclosed in epidote. Phengite is generally as discrete grains parallel to schistosity, but sometimes exhibits a decussate texture especially in pressure shadows around aggregates of chlorite and albite which are interpreted to have been garnet when the pressure shadows formed (Fig. 2h). Four fabric-parallel phengite microsamples were analysed together with three epidote grains. Phengite microsample Ph8 was extracted from the pressure shadow area adjacent to a garnet pseudomorph.

Mineral compositions

Compositional variation in white mica was investigated in a reconnaissance microprobe investigation on four of the dated samples. Small variations in phengite and paragonite content are observed in all four samples but there is no obvious correlation with microstructural setting. Representative data for 63300 have 6.78–6.96 Si per 24 O with a typical negative correlation between calculated muscovite and celadonite end-members and a weak negative correlation between celadonite and paragonite content (Fig. 4, illustrated by total Al *v.* Si and Na *v.* Si plots). The microprobe compositions are presented in Table S2. High contrast SEM images did not reveal any evidence for intragrain zoning in mean atomic number.

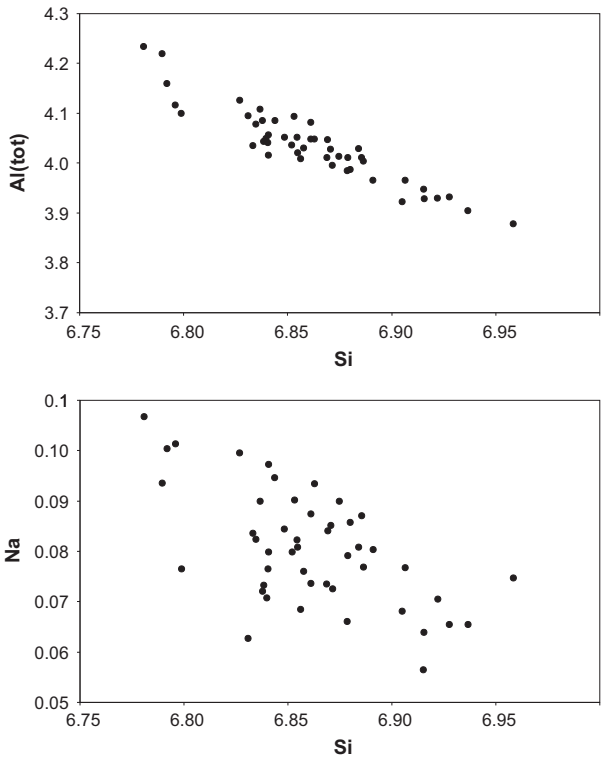

Fig. 4. Electron microprobe data for phengite from 63300 showing Al(total) and Na *v.* Si (24 O basis).

RESULTS

General features of the data set

Rb–Sr isotopic data for the analysed microsamples are presented in Table 1. Sr blanks ranged from 17 to 153 pg with a median of 40 pg; errors on $^{87}Sr/^{86}Sr$ ratios in the blanks were always large due to Rb interference on low Sr beams but were consistent with the value of 0.708 ± 0.002 assigned in the error propagation. Rubidium blanks ranged from 3 to 32 pg and were always insignificant for age calculation.

The amounts of Sr ranged from a few hundred picograms up to hundreds of nanograms; for the phengite the lowest amounts involved significant blank corrections and this produces an important increase in uncertainty in $^{87}Sr/^{86}Sr$ but it also leads to strong correlation with the $^{87}Rb/^{86}Sr$ ratio so that the effect on the age uncertainty is demagnified.

As noted above the technique used does not produce accurate concentration data; approximate ranges are listed in Table S3. Phengite has wide range of apparent concentrations, mainly reflecting the variable influence of high-Sr inclusions, chiefly epidote. Based on the approximate concentrations, the Sr mass balance for each sample can be estimated and is illustrated in Fig. 5. In most of the samples carbonate completely dominates the Sr budget and the fraction of Sr potentially isolated in phengite is <2%.

Data for individual localities

Gria Spilia

Sample 63287 is the only one in which extremely little evidence of greenschist facies overprint was observed. Microsamples from two separate polished sections were analysed. Three fresh calcite grains from both sections yielded identical Sr isotopic compositions. Four phengite grains from one section gave ages of 52.5 ± 0.8, 52.1 ± 1.1, 46.9 ± 2.3 and 28.5 ± 0.6 Ma; the three ages from the second section are more tightly grouped at 48.6 ± 0.5, 47.1 ± 0.6 and 46.2 ± 1.3 Ma. In general the texture of all seven grains is very similar, although the SEM image of phengite 6 with the youngest age does have finer grained phengite on one side; it

Table 1. Rb–Sr analytical data.

Sample	Mineral	Microsample no.	ng Rb	ng Sr	$^{87}Rb/^{86}Sr$	2s error	$^{87}Sr/^{86}Sr$	2s error	Rho[a]	Age (Ma)	2s error
63287a	Calcite	1b	nd	276	0	0	0.70892	0.00001			
Gria Spilia	Calcite	2	nd	526	0	0	0.70888	0.00001			
	Phengite	3	66	5.9	31.9	0.5	0.73272	0.00016	0.16	52.5	0.8
	Phengite	6	79	3.7	62.2	1.3	0.73409	0.00037	0.4	28.5	0.6
	Phengite	7	57	6.9	23.7	0.3	0.72641	0.00032		52.1	1.1
	Phengite	7+	63	19.4	9.29	0.44	0.7151	0.00006		46.9	2.3
63287b	Calcite	1	0.008	16	0.0015	0.00002	0.7089	0.00006			
	Calcite (altered)		4	52	0.216	0.002	0.709	0.00073			
	Phengite	5	83	6.2	38.8	0.4	0.73567	0.00018	0.33	48.6	0.5
	Phengite	6	54	4.5	35	0.4	0.7323	0.00027	0.44	47.1	0.6
	Phengite	8	15	1.6	26.1	0.5	0.72601	0.00068	0.73	46.2	1.3
63286	Calcite	1	nd	8.1	0	0	0.70826	0.00005			
Diapori	Calcite	2	nd	305	0	0	0.70815	0.00001			
	Phengite	3	14	0.2	202	27	0.8096	0.0147	0.982	35.2	1
	Phengite	4	17	0.16	309	52	0.822	0.026	0.945	26	2.3
	Phengite	6 + 8	58	1.6	104.3	2	0.7635	0.0016	0.628	37.4	0.8
	Phengite	11	26	0.18	415	57	0.911	0.029	0.987	34.4	0.8
	Phengite	17	26	0.28	274	25	0.854	0.015	0.9	37.5	1.7
63297	Calcite	5	nd	209	0	0	0.70727	0.00001			
Diapori	Calcite	6	nd	186	0	0	0.70726	0.00001			
	Calcite	7	nd	176	0	0	0.70725	0.00001			
	Phengite	1	78	11	20.5	0.2	0.71905	0.0003		40.5	1.1
	Phengite	2	96	14	20	0.2	0.71736	0.00012		35.6	0.5
	Phengite	3	92	3.6	73.5	0.8	0.74084	0.00023	0.47	32.2	0.3
	Phengite	4	54	7.9	19.6	0.2	0.71691	0.00031		34.6	1.1
	Phengite	5	140	15	26.2	0.3	0.72006	0.00012		34.4	0.5
63300	Calcite	1	nd	178	0	0	0.70771	0.00004			
Diapori	Calcite (Phengite leach)		nd	22	0	0	0.70768	0.00002			
	Phengite	1	42	0.22	573	70	1.01	0.037	0.995	37.1	0.4
	Phengite	2	105	0.85	363	12	0.9161	0.0066	0.948	40.5	0.4
	Phengite	5	40	0.3	388	17	0.938	0.021	0.974	41.8	2
	Phengite	6	20	0.17	352	54	0.912	0.035	0.986	40.9	1.3
63310	Calcite	1	bd	6.5	0	0	0.70557	0.00008			
Delfini	Calcite	2	bd	21	0	0	0.70544	0.00001			
	Epidote	1	0.5	71	0.0201	0.0001	0.705282	0.000008			
	Epidote	2	0.03	12	0.0068	0.0002	0.705371	0.00002			
	Epidote	3	nd	34	*0*	*0*	0.705319	0.000008			
	Phengite	1 + 2+5	42	3.1	39.28	0.44	0.72292	0.00014	0.257	31.3	0.4
	Phengite	7 + 8	25	1.4	50.52	0.92	0.7266	0.0008	0.174	29.5	1.2
63314	Apatite	1	0.3	14	0.062	0.001	0.70506	0.00001			
Delfini	Epidote	1	0.02	47	0.0011	0.00001	0.70546	0.00001			
	Titanite	1	2.6	4.2	1.76	0.02	0.70648	0.00012		40.9	4.9
	Titanite	2	1.7	2.1	2.35	0.03	0.70675	0.0001		38.7	2.9
	Phengite	1	16	1.2	38.57	0.48	0.72144	0.00046	0.461	29.2	0.7
	Phengite	2	38	16	6.84	0.07	0.70876	0.00017		34	1.7
	Phengite	3	6.4	12	1.55	0.02	0.70633	0.00007		39.5	3.1
	Phengite	5	17	17	2.8	0.03	0.70681	0.00004		33.9	1.2
	Phengite	6	47	4	33.5	0.35	0.71957	0.00031		29.7	0.7
	Phengite	7	42	17	7.28	0.07	0.70921	0.00014		36.3	1.3
	Phengite	8	42	5.6	21.9	0.23	0.71611	0.00037		34.3	1.2
	Phengite	9	76	26	8.46	0.08	0.70951	0.00005		33.7	0.6
S97/234	Epidote	2	0.15	44	0.0094	0.0001	0.707462	0.000014			
N. Oros Syringas	Epidote	3	0.75	134	0.016	0.002	0.707391	0.000017			
	Epidote	4	0.01	12	0.0031	0.00003	0.70806	0.00018			
	Phengite	3	6.4	0.9	20.21	0.28	0.71711	0.00003	0.308	33.6	0.4
	Phengite	4	8.3	1.1	21.94	0.28	0.71663	0.00078	0.356	29.4	2.3
	Phengite	8	127	7.7	47.9	0.5	0.72309	0.00077	0.182	23	1.1
	Phengite	9	31	0.94	93.9	3.3	0.7528	0.0019	0.945	34	0.5
63301	Calcite	1	0.07	143	0.00136	0.00001	0.71013	0.000004			
Foinikia	Calcite	2	bd	160	0.00014	0.000001	0.71013	0.00002			
	Titanite	1	0.11	12	0.0271	0.0003	0.70986	0.00002			
	Titanite	3	0.36	16	0.0624	0.0006	0.70986	0.00002			
	Phengite	1	30	30	2.94	0.03	0.71096	0.00008			
	Phengite	2	36	1024	0.1	0.01	0.7085	0.0006			
	Phengite	3	21	1.1	55.1	3.5	0.7337	0.0017	0.948	30.1	0.7
	Phengite	5 + 5a	29	1.3	65.3	3.5	0.741	0.002	0.964	33.7	0.6
	Phengite	7	42	137	0.88	0.02	0.70904	0.00068			

[a]Correlation coefficients are only listed when >0.15.

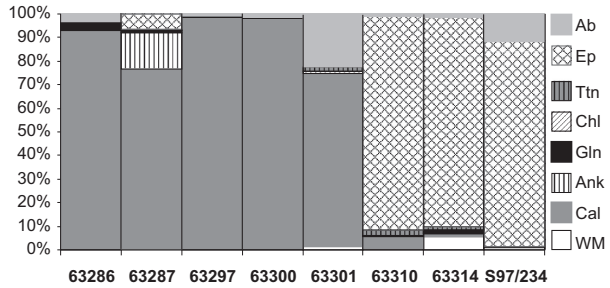

Fig. 5. Approximate Sr budgets for the analysed samples, showing the dominance of calcite and/or epidote.

is possible that such material extended into the sample volume below the surface imaged by the SEM.

Diapori

The ages of four fabric-parallel phengite grains in sample 63286 range from 37.5 ± 1.7 to 34.4 ± 0.8 Ma. Regressing all four grains plus calcite results in an elevated MSWD of 9.9 suggesting there are real differences between them. The fifth phengite from a randomly oriented aggregate has a significantly younger age of 26.0 ± 2.3 Ma.

In sample 63297 five phengite and three spatially associated calcite grains were analysed. No significant variation in $^{87}Sr/^{86}Sr$ in calcite from different microstructural positions was observed. The four fabric-parallel phengite ages ranged from 35.6 ± 0.5 to 32.2 ± 0.3 Ma. The SEM images of these phengite grains and the rather low-Rb/Sr ratios of three of them suggest their compositions might be biased by inclusions of epidote. However, regressing the four grains on their own results in a slightly elevated initial ratio (0.7086 cf. 0.7072) rather than a lower value as expected if older inclusions were causing bias. The joint age produced by this calculation is 30.9 ± 0.5 Ma (MSWD = 1.3) but this is not likely to be geologically significant. A slightly older age of 40.5 ± 1.1 Ma for the fifth phengite is consistent with the observed microstructural relationship in which it is wrapped by fabric-parallel grains (Fig. 3c).

Four fabric-parallel phengite grains from sample 63300 gave ages between 41.8 ± 2.0 and 37.1 ± 0.4 Ma again using calcite to estimate the initial Sr composition. Three of these are consistent within error of a pooled age of 40.5 ± 0.4 Ma; the fourth is significantly younger.

Delfini

The two composite phengite grains from sample 63310 gave ages of 31.3 ± 0.4 and 29.5 ± 1.2 Ma using the calcite analyses to estimate the initial Sr. The epidote $^{87}Sr/^{86}Sr$ is slightly lower suggesting it did not fully re-equilibrate during fabric development but the age would not change significantly if epidote were used in the age calculation instead of calcite.

In sample 63314 eight phengite microsamples were analysed. They exhibit a wide range of apparent $^{87}Rb/^{86}Sr$ ratios between 1.5 and 39; this is consistent with the SEM observations that show abundant small epidote inclusions inside phengite grains that could not be completely avoided by microsampling. The two grains with the highest $^{87}Rb/^{86}Sr$ gave ages of 29.2 ± 0.7 and 29.7 ± 0.7 Ma (29.4 ± 0.5 Ma weighted mean age). The remaining six grains have ages ranging from 39.5 ± 3.1 to 33.9 ± 1.2 Ma; regressing them together with the epidote analysis gives an age of 34.2 ± 1.3 Ma (MSWD = 4.9). For these six there is no clear relationship between $^{87}Rb/^{86}Sr$ and apparent age.

Analysis of two titanite microsamples, incorporating their phengite inclusions, showed significant radiogenic enrichment above the epidote and apatite; regressing these with the epidote gives an age of 39.3 ± 2.5 Ma (MSWD 0.59), older than the individual phengite outside the titanite grains.

Oros Syringas

In sample S97/234 four phengite microsamples were analysed together with three epidote. One of the latter has a slightly elevated $^{87}Sr/^{86}Sr$ compared to the other two, but the difference would have no significant impact on calculated phengite ages. The phengite ages range from 34.0 ± 0.5 to 23.0 ± 1.1 Ma. There is no obvious textural distinction between the youngest age and the other three which are more tightly grouped with a pooled age 33.9 ± 1.8 Ma (MSWD 6.6).

Foinikia

Three of the five analysed phengite grains from sample 63301 have high Sr contents and $^{87}Rb/^{86}Sr$ too low for reliable age calculation. The remaining two give ages of 30.1 ± 0.7 and 33.7 ± 0.6 Ma when tied to an initial ratio based on the calcite analyses. Use of the slightly lower titanite compositions does not change the ages significantly. Texturally the older age relates to a cluster of mica grains sub-parallel to the schistosity whereas the microsample with the younger age was from a radiating cluster at a high angle to the fabric.

DISCUSSION

The temperatures involved along the *P–T–t* paths followed by the CBB remained below those required for significant diffusive equilibration of white mica as discussed above. The following discussion is therefore based on the interpretation that variation in white mica ages presented here are not controlled by

cooling history. It is important also to consider whether variations in apparent age might be due to use of inappropriate initial Sr isotopic composition. As emphasized by the recent study by Sousa *et al.* (2013), at any specific time in the microstructural development of a rock the Sr incorporated into growing minerals may not have the same isotopic composition as the whole rock at that time. To minimize any bias resulting from this effect, microsamples of low-Rb/Sr minerals in close proximity to the analysed white mica were analysed. In most cases these were from minerals that are interpreted as having actively re-crystallized with the mica. For individual samples we did not observe any differences between the different microsamples of calcite or epidote in each section at a level that would significantly influence the calculated phengite age. In all but two samples calcite was analysed and, as noted above, was a major contributor to the overall Sr mass balance; carbonate accounts for >90% of the Sr budget in the calcschists (Fig. 5). The modal abundance of calcite in the greenschist sample from Foinikia (63301) is only ~10% but it still accounts for three quarters of the Sr. In the other greenschist sample (S97/234, from Oros Syringas), and in the samples from Delfini, epidote contains ~90% of the Sr budget. Therefore, we consider it unlikely that uncertainties over the appropriate initial Sr composition are a major cause of variation in the calculated ages.

The extent to which the wide range of mineral ages found in previous studies can be interpreted in terms of specific crystallization events was recently discussed by Bröcker *et al.* (2013). They concluded that actual ages of crystallization were masked by some combination of partial resetting of older ages and mixing of different generations of mica. They also noted a significant range in major element composition of white mica in their samples. Bröcker *et al.* (2013) were not able to determine the relative importance of these effects because their own and earlier data were measured on separated mineral fractions. If mixing of different generations is the dominant effect then the approach presented here, using microsamples from specific microstructural settings, should reveal whether distinct generations of white mica are present at the thin-section scale.

Timing and duration of blueschist conditions

The significance of the results from the various locations on Syros are now discussed in turn.

Gria Spilia

Sample 63287 is from the garnet–glaucophane calcschist matrix of the conglomerate and has only very minor retrogression, evidenced by fine-grained plagioclase intergrown with other phases. This sample yielded the oldest ages. Excluding phengite microsample 6 (Table 1), which may be affected by fine-grained retrogressive phengite, the age range from 53 to 47 Ma is similar to previous results from the very northern part of Syros, north of the Serpentinite Belt (Fig. 1). Bröcker & Enders (2001) reported Rb–Sr ages of 49.4 ± 0.7 and 46.4 ± 0.7 Ma for phengite in two omphacite-bearing boulders. Lagos *et al.* (2007) reported Lu–Hf garnet ages of 52.2 ± 0.3 and 51.4 ± 0.4 Ma and Tomaschek *et al.* (2003) found a 52.4 ± 0.8 Ma zircon generation in a plagiogranite which they attributed to crystallization from a high-*P* metamorphic fluid. These ages are all from relatively competent lithologies; the more ductile calcschists dated here may have continued to take up later deformation explaining the spread to somewhat younger ages, which range down to 45 Ma in the mica dated here.

Diapori

Peak temperatures recorded south of the Serpentinite Belt were estimated to be <510 °C (Schumacher *et al.*, 2008). Ages from Diapori are summarized in Fig. 6a. The three samples of calcschist matrix from the conglomerate provide the clearest evidence that ages from different generations of phengite are preserved on the scale of a single thin section. Seven of the analysed microsamples are from fabric-parallel phengite grains and have analytical precision below 1 Ma; the ages span from 40.5 ± 0.4 to 32.2 ± 0.3 Ma. Another five have poorer precision but do not significantly expand the age range. One microsample from sample 63297 is from a grain oriented at a high angle to the schistosity; fabric-parallel phengite wraps around this grain. The age of the texturally earlier grain is 40.5 ± 1.1 Ma, which is slightly older than the fabric-parallel ages in this sample which do not exceed 35.6 ± 0.5 Ma. In 63286, on the other hand, the fabric-parallel phengite with an age of 35.2 ± 1.0 Ma is located <1 mm away from the finer grained randomly oriented aggregate sampled as phengite 4 which has a significantly younger age of 26.0 ± 2.3 Ma (Fig. 6a). The distinct ages of the texturally oldest and youngest microsamples suggest how the spread in ages of the fabric-parallel phengite microsamples should be interpreted; they extend up to (and beyond) that of the texturally oldest age. This implies that the generation of the dominant fabric involved significant passive rotation of pre-existing phengite, accompanied by variable re-crystallization/crystallization of new grains parallel to the fabric. While the oldest grains crystallized *c.* 40 Ma, the youngest did so at *c.* 32 Ma. The development of the finite deformation fabric had a protracted history that was not completed until this younger age, or later. Blueschist facies conditions and associated deformation continued over a

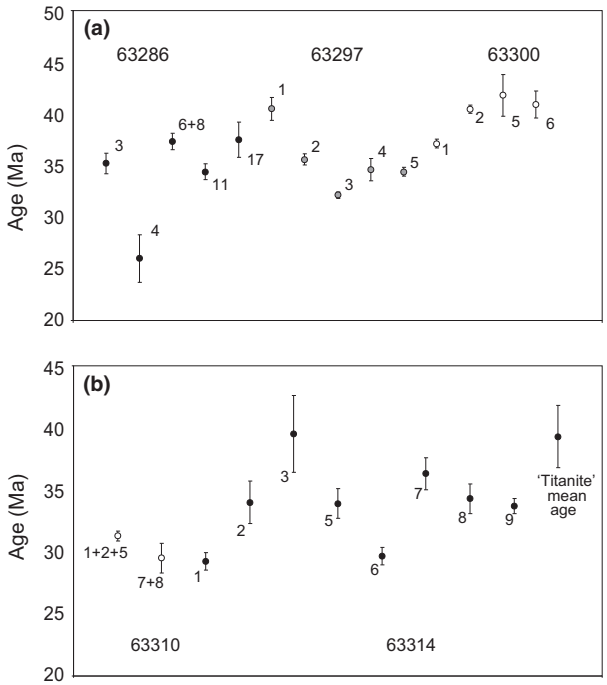

Fig. 6. (a) Summary of phengite Rb–Sr ages for Diapori sub-area; (b) summary of phengite Rb–Sr ages for Delfini sub-area.

protracted period of at least 8 Ma. There is no clear evidence in these three samples of deformation continuing into the greenschist facies, since both albite crystallization and the, probably pseudomorphic, 26 Ma randomly oriented phengite appear to be post-tectonic. Unfortunately none of the samples from greenschist rocks that overlie the conglomeratic unit at Diapori contained phengite large enough for microsampling and thus remain undated.

Delfini

The ages for this area are summarized in Fig. 6b. The phengite in 63310 is associated with bent or fractured, generally unretrogressed blue amphibole in a fabric that wraps around larger epidote grains. This suggests phengite crystallization under blueschist facies conditions. The ages obtained here, of 31.3 and 29.5 Ma, imply these conditions persisted until *c*. 30 Ma. This result is consistent with the interpretation of the data from Diapori. However, the data from sample 63314 present a more complex picture. Overall data quality is limited by abundant tiny epidote inclusions in the phengite (Fig. 3e,f) that result in a wide range of Rb/Sr ratios even in carefully selected microsamples. The ages from the two microsamples with the highest Rb/Sr ratios are considered most reliable and these indicate an age of 29.4 ± 0.5 Ma in agreement with the data from sample 63310. However, there is evidence for an older generation of phengite which defines an internal fabric within titanite grains. Analyses of two titanite microsamples show elevated Rb/Sr ratios reflecting the presence of the early phengite inclusions. The mean apparent age of these titanite–phengite composites is 39.3 ± 2.5 Ma confirming that phengite crystallized over a period on the order of 10 Ma in this sample. Again this confirms protracted deformation and crystallization/recrystallization under blueschist conditions deduced from the Diapori samples. The apparently older age, close to 34 Ma, of the less precise phengite microsample ages may reflect a real range in ages rather than bias due to the enhanced sensitivity of low-Rb/Sr ages to initial ratio uncertainties.

Summary

The ages of fabric-forming phengite in the blueschist facies samples from Syros presented here range from 53 to 30 Ma. In some of the dated samples blue amphibole was cracked during extension as the fabric developed without significant retrogression. Indeed sample 63314 contains new blue amphibole that grew into cracks in older blue amphibole. These textural observations of repeated fracturing and crystallization of blue amphibole are consistent with deformation under blueschist facies persisting as late as 30 Ma.

Timing of greenschist facies overprint

Two of the samples reported here are dominated by greenschist facies assemblages. Only two of the five phengite microsamples from 63301 have high enough Rb/Sr for precise age calculation. One was from a cluster of grains sub-parallel to the schistosity that yielded an age of 33.7 ± 0.6 Ma. This is indistinguishable from the majority of ages from blueschist facies assemblages. Consequently the age is likely to reflect survival of phengite from an earlier blueschist facies stage in the metamorphic history. A younger age (30.1 ± 0.7 Ma) was determined on a decussate cluster of grains which probably post-dates fabric-forming deformation. There is no clear indication whether this formed under greenschist facies conditions. The four ages from fabric-parallel phengite in sample S97/234 show a wide spread in age from 34 to 23 Ma with no obvious differences in microstructural setting. This sample contains chlorite pseudomorphs after garnet. The spread in ages is considered to reflect a fabric which includes both relicts from the earlier higher grade assemblage and phengite newly crystallized under greenschist facies conditions.

Overall the timing of the transition to greenschist facies conditions and deformation under such conditions remains poorly dated. It is bracketed by the post-tectonic ages of 26 Ma for sample 63286, and the youngest blueschist facies ages which extend down to 29 Ma. That some deformation occurred

under greenschist facies conditions is documented by the microstructures in samples 63298 and 63299 described above (see also Bond *et al*., 2007).

Timing and duration of sub-horizontal extension

The dominant fabric in all of the dated samples is related to exhumation by low-angle extensional deformation described by Bond *et al*. (2007). Our age data support the models of Philippon *et al*. (2011) and Laurent *et al*. (2016) which link (dashed line in Fig. 1), the east–west-trending Serpentinite Belt that crosses the northern part of Syros, with a north–south-oriented discontinuity that places the northern tip of Syros (Diapori) stratigraphically below the Serpentinite Belt. North of the Serpentinite Belt this deformation was under way by 53 Ma. Further south such deformation was in progress by *c*. 40 Ma and continued under blueschist facies conditions until *c*. 29 Ma. Exhumation continued into the greenschist facies and was locally completed by 25 Ma when post-tectonic greenschist facies mica crystallized.

Punctuated *v*. continuous deformation

This study aimed to determine whether metamorphic terranes, such as that exposed on Syros, are the result of continuously evolving metamorphic and tectonic processes, or result from a series of punctuated events. This ambition was not conclusively achieved for a variety of reasons although the results are quite consistent with continuously evolving processes as exhumation progressed. Field and thin section observations from this study and that of Bond *et al*. (2007) suggest that recrystallization to lower pressure and temperature phases was localized by factors including deformation localization and non-pervasive fluid so that minerals crystallized at different metamorphic grades occur in close proximity within single samples. The *P–T* conditions changed through blueschist facies between 54 and 30 Ma eventually passing into the greenschist facies by *c*. 25 Ma. This scenario accords with previously published age ranges (Baldwin, 1996; Bröcker & Enders, 2001; Ring & Layer, 2003; Tomaschek *et al*., 2003; Putlitz *et al*., 2005; Lagos *et al*., 2007; Bröcker *et al*., 2013; Rogowitz *et al*., 2015, see Table S1 for summary details of the dating featured in these papers).

Despite intensive geochronological investigation, involving 39 white mica ages from a suite of eight samples, in addition to the numerous dates from other studies (e.g. Bröcker & Enders, 1999, 2001; Bröcker *et al*., 2004; Keiter *et al*., 2004; see also Table S1) the initial questions posed in this study remain to be conclusively answered and it is evident that a much larger number of dates from carefully targeted samples would be required if further progress is to be made.

CONCLUSIONS

A suite of new Rb–Sr phengite ages has been obtained on microsamples from defined microstructural settings on Syros. They reveal a complex pattern in which ages vary between different settings at thin-section scale. The data set provides no support for deformation and mica crystallization in discrete regionally significant episodes; rather they are consistent with continuous deformation whose locus migrated within the crust on a small scale as metamorphism and deformation modified the rheological properties at scales down to individual rock specimens as proposed by Bond *et al*. (2007).

The ages indicate that crystallization under blueschist facies conditions occurred in the interval from 53 to 29 Ma, accompanying low-angle extensional deformation later culminating in deformation in the greenschist facies. Two phengite microsamples give 26–23 Ma ages consistent with previous data on the timing of greenschist facies.

Our new results show it is possible to extract mica with masses of only a few hundred micrograms, sometimes with <1 ng Sr, and obtain ages with useful analytical precision. The coexistence of phengite of different ages at thin-section scale has been confirmed, so that ages reported utilizing conventional mineral separates inevitably yield mixed ages. To obtain tectonically meaningful results it is essential to analyse samples related to microstructure on the microscopic scale. Even then mechanical rotation of older grains into new deformation fabrics may result in ages that are older than the observed deformation.

Given heterogeneity in the localization of deformation across a terrane, a much larger data set would be required to detect any concentration of deformation in distinct 'episodes'. To sample and date sufficient samples that can be clearly tied microstructurally to defined deformation events across the terrane would demand substantial effort and resources, especially given the small proportion (<10%) of samples that ultimately provide useable ages. However, existing data are compatible with tectonic models that invoke continuous deformation in both space and time, as might be expected at plate boundaries. They do not support the notion of tectonics progressing through a series of discrete events punctuated in time.

ACKNOWLEDGEMENTS

This work was funded by NERC grant NE/D008263/1 ('Punctuated or continuous deformation during the exhumation of subducted crust? A linked tectono-metamorphic and geochronological study'). Thanks for assistance to C. Rogers with the Rb–Sr analysis and to E. Condliffe with SEM work in Leeds. Use of the Edinburgh Materials and Micro-Analysis Centre by one of

us (JED) is gratefully acknowledged. A. Smye and S. Reddy are thanked for their helpful reviews. This paper was completed after the death of our colleague and friend, John 'JED' Dixon, who passed away in 2013.

REFERENCES

Anczkiewicz, R. & Thirlwall, M.F., 2003. Improving precision of Sm–Nd garnet dating by H_2SO_4 leaching: a simple solution to the phosphate inclusion problem. *Geological Society, London, Special Publications*, **220,** 83–91.

Baldwin, S.L., 1996. Contrasting P-T-t Histories for Blueschists from the Western Baja Terrane and the Aegean: Effects of Synsubduction Exhumation and Backarc Extension. In: *Subduction Top to Bottom, Geophysical Monographs*, **96,** pp. 135–141.

Bond, C.E., Butler, R.W.H. & Dixon, J.E., 2007. Co-axial horizontal stretching within extending orogens: the exhumation of HP rocks on Syros (Cyclades) revisited. *Geological Society Special Publication*, **272,** 203–222.

Bonneau, M. 1984. Correlation of the Hellenide nappes in the south–east Aegean and their tectonic reconstruction. In: *The Geological Evolution of the Eastern Mediterranean* (eds Dixon, J.E. & Robertson, A.H.F.), *Geological Society, London, Special Publications*, **17,** 517–527.

Brady, J.B., Markley, M.J., Schumacher, J.C., Cheney, J.T. & Bianciardi, G.A., 2004. Aragonite pseudomorphs in high-pressure marbles of Syros, Greece. *Journal of Structural Geology*, **26,** 3–9.

Bröcker, M. & Enders, M., 1999. U-Pb zircon geochronology of unusual eclogite-facies rocks from Syros and Tinos, Cyclades, Greece. *Geological Magazine*, **136,** 111–118.

Bröcker, M. & Enders, M., 2001. Unusual bulk-rock compositions in eclogite-facies rocks from Syros and Tinos (Cyclades, Greece): implications for U-Pb zircon geochronology. *Chemical Geology*, **175,** 581–603.

Bröcker, M. & Keasling, A., 2006. Ionprobe U-Pb zircon ages from the high-pressure/low-temperature mélange of Syros, Greece: age diversity and the importance of pre-Eocene subduction. *Journal of Metamorphic Geology*, **24,** 615–631.

Bröcker, M., Bieling, D., Hacker, B. & Gans, P., 2004. High-Si phengite records the time of greenschist-facies overprinting: implications for models suggesting mega-detachments in the Aegean Sea. *Journal of Metamorphic Geology*, **22,** 427–442.

Bröcker, M., Baldwin, S. & Arkudas, R., 2013. The geological significance of $^{40}Ar/^{39}Ar$ and Rb–Sr white mica ages from Syros and Sifnos, Greece: a record of continuous (re)crystallization during exhumation? *Journal of Metamorphic Geology*, **31,** 629–646.

Cherniak, D.J., 1997. An experimental study of strontium and lead diffusion in calcite, and implications for carbonate diagenesis and metamorphism. *Geochimica et Cosmochimica Acta*, **61,** 4173–4179.

Cliff, R.A. & Meffan-Main, S., 2003. Evidence from Rb–Sr microsampling geochronology for the timing of Alpine deformation in the Sonnblick Dome, SE Tauern Window, Austria. In: *Geochronology: Linking the Isotopic Record with Petrology and Textures* (eds Vance, D., Muller, W. & Villa, I.M.), *Geological Society of London, Special Publications*, **220,** 159–172.

Cliff, R.A., Rex, D.C. & Droop, G.T.R., 1985. Alpine metamorphism in the south–east Tauern Window, Austria; 2. Rates of heating, cooling and uplift. *Journal of Metamorphic Geology*, **3,** 403–415.

Dixon, J.E., 1976. Glaucophane schists of Syros, Greece. *Bulletin de la Societé Géologique de France*, **7,** 280.

Dixon, J.E., Feenstra, A., Jansen, J.B.H. *et al.*, 1987. *Excursion guide to the field trip on Seriphos, Syros and Naxos*. In: *Chemical Transport in Metasomatic Processes* (ed. Helgeson, H.C.), pp. 218–518. NATO ASI Series.

Droop, G.T.R., 1985. Alpine metamorphism in the south–east Tauern Window, Austria; 1. P-T variations in space and time. *Journal of Metamorphic Geology*, **3,** 371–402.

Erickson, T.M., Pearce, M.A., Taylor, R.J.M. *et al.*, 2015. Deformed monazite yields high-temperature tectonic ages. *Geology*, **43,** 383–386.

Forster, M.A. & Lister, G.S., 2005. Several distinct tectonometamorphic slices in the Cycladic eclogite–blueschist belt, Greece. *Contributions to Mineralogy and Petrology*, **150,** 523–545.

Freeman, S.R., Inger, S., Butler, R.W.H. & Cliff, R.A., 1997. Dating deformation using Rb–Sr in white mica: greenschist facies deformation ages from the Entrelor shear zone, Italian Alps. *Tectonics*, **16,** 57–76.

Fu, B., Valley, J.W. & Kita, N.T., 2010. Multiple origins of zircons in jadeitite. *Contributions to Mineralogy and Petrology*, **159,** 769–780.

Ganor, J., Matthews, A. & Paldor, N., 1989. Constraints on effective diffusivity during oxygen isotope exchange at a marble–schist contact, Sifnos (Cyclades), Greece. *Earth and Planetary Science Letters*, **94,** 208–216.

Jäger, E., Niggli, E. & Wenk, E., 1967. *Rb–Sr Altersbestimmungen an Glimmern der Zentralalpen. Beiträge Zur Geologische Karte der Schweiz, N.F. 134*. Kümmerly & Frey, Bern, 67 pp.

Jenkin, G.R.T., Rogers, G., Fallick, A.E. & Farrow, C.M., 1995. Rb–Sr closure temperatures in bi-mineralic rocks; a mode effect and test for different diffusion models. *Chemical Geology* (Isotope Geoscience Section), **122,** 227–240.

Jolivet, L., Goffé, B., Bousquet, R., Oberhansli, R. & Michard, A., 1998. Detachments in high-pressure mountain belts, Tethyan examples. *Earth and Planetary Science Letters*, **160,** 31–47.

Keiter, M., Piepjohn, K., Ballhaus, C., Lagos, M. & Bode, M., 2004. Structural development of high-pressure metamorphic rocks on Syros Island (Cyclades, Greece). *Journal of Structural Geology*, **26,** 1433–1445.

Lagos, M., Scherer, E.E. & Tomaschek, F., 2007. High precision Lu–Hf geochronology of Eocene eclogite-facies rocks from Syros, Cyclades, Greece. *Chemical Geology*, **243,** 16–35.

Laurent, V., Jolivet, L., Roche, V., Augier, R., Scaillet, S. & Cardello, G.L., 2016. Strain localization in a fossilized subduction channel: insights from the Cycladic Blueschist Unit (Syros, Greece). *Tectonophysics*, **672,** 150–169.

Lister, G.S., Banga, G. & Feenstra, A., 1984. Metamorphic core complexes of Cordilleran type in the Cyclades, Aegean Sea, Greece. *Geology*, **12,** 221–225.

Ludwig, K.R., 2012. A geochronological toolkit for microsoft excel. Berkeley Geochronology Center Special Publication, No. 5, 76 pp.

Mottram, C.M., Parrish, R.R., Regis, D. *et al.*, 2015. Using U-Th–Pb petrochronology to determine rates of ductile thrusting: time windows into the Main Central Thrust, Sikkim Himalaya. *Tectonics*, **34,** 1355–1374.

Okrusch, M. & Bröcker, M., 1990. Eclogite facies rocks in the Cycladic blueschist belt, Greece: a review. *European Journal of Mineralogy*, **2,** 451–478.

Philippon, M., Brun, J. P. & Gueydan, F., 2011. Tectonics of the Syros blueschists (Cyclades, Greece); from subduction to Aegean extension. *Tectonics*, **30,** DOI: 10.1029/2010TC002810.

Philippon, M., Gueydan, F., Pitra, P. & Brun, J.-P., 2013. Preservation of subduction-related prograde deformation in lawsonite pseudomorph-bearing rocks. *Journal of Metamorphic Geology*, **31,** 571–583.

Putlitz, B., Cosca, M.A. & Schumacher, J.C., 2005. Prograde mica $^{40}Ar/^{39}Ar$ growth ages recorded in high pressure rocks (Syros, Cyclades, Greece). *Chemical Geology*, **214,** 79–98.

Ridley, J.R., 1982. Arcuate lineation trends in a deep level ductile thrust belt, Syros, Greece. *Tectonophysics*, **88,** 347–360.

Ring, U. & Layer, P.W., 2003. High-pressure metamorphism in the Aegean, eastern Mediterranean: Underplating and exhumation from the Late Cretaceous until the Miocene to Recent above the retreating Hellenic subduction zone. *Tectonics*, **22,** DOI:10.1029/2001TC001350.

Roddick, J.C., Cliff, R.A. & Rex, D.C., 1980. The isotopic evolution of excess argon in some Alpine biotites. *Earth and Planetary Science Letters*, **48,** 185–208.

Rogowitz, A., Huet, B., Schneider, D. & Grasemann, B., 2015. Influence of high strain rate deformation on $^{40}Ar/^{39}Ar$ mica ages from marble mylonites (Syros, Greece). *Lithosphere*, **7,** 535–540.

Rosenbaum, G., Avigad, D. & Sanchez-Gomez, M., 2002. Coaxial flattening at deep levels of orogenic belts: evidence from blueschists and eclogites on Syros and Sifnos (Cyclades, Greece). *Journal of Structural Geology*, **24,** 1451–1462.

Scherer, E.E., Cameron, K.L. & Blichert-Toft, J., 2000. Lu–Hf garnet geochronology: closure temperature relative to the Sm–Nd system and the effects of trace mineral inclusions. *Geochimica et Cosmochimica Acta*, **64,** 3413–3432.

Schliestedt, M. & Matthews, A., 1987. Transformation of blueschist to greenschist facies rocks as a consequence of fluid infiltration, Sifnos (Cyclades), Greece. *Contributions to Mineralogy and Petrology*, **97,** 237–250.

Schumacher, J., Brady, J.B., Cheney, J.T. & Tonnsen, R.R., 2008. Glaucophane-bearing marbles on Syros, Greece. *Journal of Petrology*, **49,** 1667–1686.

Smye, A.J., Warren, C.J. & Bickle, M.J., 2013. The signature of devolatisation: extraneous ^{40}Ar systematics in high-pressure metamorphic rocks. *Geochimica et Cosmochimica Acta*, **113,** 94–112.

Soukis, K. & Stockli, D.F., 2013. Structural and thermochronometric evidence for multi-stage exhumation of southern Syros, Cycladic islands, Greece. *Tectonophysics*, **595–596,** 148–164.

Sousa, J., Kohn, M.J., Schmitz, M.D., Northrup, C.J. & Spear, F.S., 2013. Strontium isotope zoning in garnet; implications for metamorphic matrix equilibration, geochronology and phase equilibrium modelling. *Journal of Metamorphic Geology*, **31,** 437–452.

Tomaschek, F., Kennedy, A.K., Villa, I.M., Lagos, M. & Ballhaus, C., 2003. Zircons from Syros, Cyclades, Greece – recrystallization and mobilization of zircon during high-pressure metamorphism. *Journal of Petrology*, **44,** 1977–2002.

Trotet, F., Jolivet, L. & Vidal, O., 2001. Tectono-metamorphic evolution of Syros and Sifnos (Cyclades, Greece). *Tectonophysics*, **338,** 179–206.

Villa, I.M., 1998. Isotopic closure. *Terra Nova*, **10,** 42–47.

Warren, C.J., Smye, A.J., Kelley, S.P. & Sherlock, S.C., 2012. Using white mica $^{40}Ar/^{39}Ar$ data as a tracer for fluid flow and permeability under high-P conditions; Tauern Window, Eastern Alps. *Journal of Metamorphic Geology*, **30,** 63–80.

SUPPORTING INFORMATION

Additional Supporting Information may be found in the online version of this article at the publisher's web site:

Appendix S1. Microsample processing procedure.

Table S1. Geochronological review.

Table S2. Compositions data for Sample 63300 phengites.

Table S3. Approximate Sr concentrations.

Figure S1. Localities for greenschist-facies samples referred to in the main text in relation to the dated blueschist facies sample 63297.

Received 20 July 2016; revision accepted 17 October 2016.